Available online at www.sciencedirect.com
ScienceDirect
Acta Materialia 58 (2010) 85–91
Acta MATERIALIA
www.elsevier.com/locate/actamat

Transformation potential predictions for the stress-induced austenite to martensite transformation in steel

A. Creuziger *, T. Foecke

National Institute of Standards and Technology (NIST), 100 Bureau Drive, Gaithersburg, MD 20899, USA

Received 29 May 2009; received in revised form 24 August 2009; accepted 27 August 2009
Available online 28 September 2009

Abstract

The stress-induced transformation behavior of retained austenite is considered in this work. With the development of transformation-induced plasticity (TRIP) steels this deformation mode is of growing importance. Twinned martensite structures were calculated using the crystallographic theory of martensite. An available work criterion was used to predict the transformation potentials for 16 different in-plane stress states for sheet sample geometry. By rotating the twinned martensite structures over all crystallographic orientations using Euler angles, the magnitude of the transformation potential was plotted as an orientation distribution plot for comparison with typical texture components. From these data, the Brass and Copper orientation components that are typical in retained austenite such as in TRIP steels were found to have low transformation potential values. Grains aligned with these orientations would require higher stresses to transform than other orientations, and may therefore never transform. This correlates to experimental observations that heavily deformed TRIP steel contains residual retained austenite.
Published by Elsevier Ltd. on behalf of Acta Materialia Inc.

Keywords: TRIP steel; Texture; Austenitic steels; Martensitic phase transformation

1. Background

1.1. TRIP steel

Transformation-induced plasticity (TRIP) steels are a relatively new class of advanced high-strength steels (AHSS) that show both high strength and high ductility [1] and are being considered for widespread use in automotive applications to lighten automobile bodies. High strength and high ductility are typically mutually exclusive, but are obtained in TRIP steels by stabilization of the austenite phase and strain-induced deformation from the retained austenite into the martensite phase, as was first published by [2]. There are two categories of TRIP steels, TRIP-H and TRIP-L [3], also referred to as TRIP steel and TRIP-assisted steel, respectively [4]. TRIP-H steels are almost entirely austenite, due to high volume fractions (≈10% mass fraction) of Ni and Cr added for austenite stabilization. These high-alloy steels are fairly expensive due to the addition of these alloy elements, and have not been widely used in automotive applications [3]. In comparison, the TRIP-L steels are initially a mixture of ferrite, bainite and austenite, with the austenite composing (5–25)% of the total mass fraction depending on alloying elements and thermomechanical treatment [5]. For these alloys, the austenite is stabilized by additions of ≈2% mass fraction Mn and ≈2% mass fraction Al or Si, making these low-alloy steels [6,7]. The lower cost of the TRIP-L steels has lead to interest in use of these materials in automotive production. However, the lack of knowledge about the forming behavior in multiaxial strain states has limited the automotive use of these alloys.

This paper focuses on the crystallographic texture of the austenite phase and its effect on the transformation behavior. Prior investigations into the texture of the austenite phase [8,9] showed that the initial texture exhibits Brass

* Corresponding author. Tel.: +1 301 975 6015.
E-mail addresses: adam.creuziger@nist.gov (A. Creuziger), tim.foecke@nist.gov (T. Foecke).

1359-6454/$36.00 Published by Elsevier Ltd. on behalf of Acta Materialia Inc.
doi:10.1016/j.actamat.2009.08.059

or Copper orientations, typical for rolled face-centered cubic (FCC) materials. Materials with FCC structure also tend to recrystallize in cube orientation [10, page 221;11]. However, there has been little data on how favorable any of these orientations are to transformation.

Stress-induced martensite can transform into two possible structures: a single variant of martensite or twinned martensite. Transformation into a single variant of martensite is rare, due to the specific requirements on the lattice parameters needed for transformation [12]. However, twinned martensite has been observed in both TRIP-H steels [13] and TRIP-L steels [14].

There have been a few attempts at predicting the dependence of the orientation on transformation. Van Rompaey et al. [15] used the single-variant assumption, finite element analysis (FEA) and analytic solutions to calculate the mechanical driving force energy under multiaxial loading conditions, suggesting the use of a twinned martensite technique to advance their analysis. Zhang et al. [16] also assumed a single-variant transformation, and for uniaxial compression loading predicts that cube orientations will transform first. More detailed transformation analysis, including the difference between Kurdjumov–Sachs (K-S) and Nishiyama–Wasserman (N-W) was performed in Ref. [9], but the stress state was not taken into account.

In this work, twinned martensite structures are used, in conjunction with calculation of a transformation potential, defined below, which includes the stress required for transformation. Sixteen different in-plane stress states are applied to the twinned martensite structures. The twinned martensite structures are rotated over all of orientation space to represent possible grain orientations. This technique allows simultaneous investigation of the stress state and orientation dependence on the austenite to twinned martensite transformation and will provide a more complete view of what orientations and stress states are favorable for transformation.

1.2. Crystallographic theory of martensite

To calculate the twinned martensite structure, the crystallographic theory of martensite (CTM) was used. The full details of this method are described in Refs. [12,17,18]. The terms a' and c' are defined to be the body-centered tetragonal (BCT) unit cell dimensions, and a_0 is defined as the FCC unit cell length. For this analysis, the FCC lattice is assumed to be in the $m3m$ space group and is taken to be the reference lattice. Using these definitions, for the FCC to BCT transformation, three stretch tensors or martensite variants are possible:

$$U_1 = \begin{bmatrix} \gamma & 0 & 0 \\ 0 & \alpha & 0 \\ 0 & 0 & \alpha \end{bmatrix}, \quad U_2 = \begin{bmatrix} \alpha & 0 & 0 \\ 0 & \gamma & 0 \\ 0 & 0 & \alpha \end{bmatrix},$$
$$U_3 = \begin{bmatrix} \alpha & 0 & 0 \\ 0 & \alpha & 0 \\ 0 & 0 & \gamma \end{bmatrix}, \quad \alpha = \frac{2a'}{\sqrt{2}a_0}, \quad \gamma = \frac{c'}{a_0} \tag{1}$$

To calculate twinning, two variants labeled $\mathbf{U}^{(i)}$ and $\mathbf{U}^{(j)}$ are used as well as a rotation $\mathbf{R}$ of the martensite variant (j) in the following compatibility equation:

$$\mathbf{R}\mathbf{U}^{(j)} - \mathbf{U}^{(i)} = \mathbf{a} \otimes \hat{\mathbf{n}} \tag{2}$$

where $\mathbf{a}$ is the shearing vector of the twin and $\hat{\mathbf{n}}$ is the mirror plane normal between variants. The Bain transformation is assumed in the current analysis; the additional details of K-S or N-W transformations are not included in the twinning calculation. These transformations could be included, but most texture data is described in 5° increments, which makes the N-W and K-S transformations difficult to distinguish from the Bain transformation [19].

After the twinning equation is calculated, an additional compatibility equation between the twinned martensite and the austenite is required. The terms $\mathbf{U}^{(i)}, \mathbf{U}^{(j)}, \mathbf{R}$ terms are the same as used in Eq. (2), with the additional terms for the rotation of the twinned structure $\bar{\mathbf{R}}$ for compatibility with the austenite $\mathbf{I}$ and the variant volume ratio λ describing the relative proportion of the two martensite variants in the twinned structure. The compatibility equation for an austenite-twinned martensite interface is:

$$\overline{\mathbf{R}}\left(\lambda \mathbf{R}\mathbf{U}^{(\mathbf{j})} + (\mathbf{1}-\lambda)\mathbf{U}^{(\mathbf{i})}\right) - \mathbf{I} = \mathbf{b} \otimes \hat{\mathbf{m}} \tag{3}$$

The austenite to twinned martensite interface can thus be described as two vectors, containing the plane normal to the interface $\hat{\mathbf{m}}$ and the shearing direction and magnitude $\mathbf{b}$ for the twinned structure. For the FCC $m3m$ point group and the BCT 23 point group in Hermann–Mauguin notation, there are 24 possible interfaces. A program developed by T.W. Shield was used for these calculations [20].

1.3. Available work criterion

In order to predict which of the twinned martensite structures are likely to form, an available work criterion is applied:

$$W^{(k)} = \mathrm{b}_i^{(k)} \sigma_{ij} \hat{\mathrm{m}}_j^{(k)} \tag{4}$$

where b and $\hat{\mathrm{m}}$ are the interface vectors for the 24 possible interfaces (k) and σ is the stress state. The scalar W represents the value of a transformation potential and is derived from the Schmid law for plasticity and is similar to the critical resolved shear stress [21]. For a given stress state, the maximum value of $W^{(k)}$ for all k is denoted as $\widetilde{W}$. The interface associated with the maximum value $\widetilde{W}$, defined as $\tilde{k}$, is the interface that is most likely to form. This criterion has been used previously to predict the specific twinned martensite structure that forms in both uniaxial tension and around a notch in shape-memory alloys with good agreement [21–23]. To avoid confusion when discussing the magnitudes of the maximum transformation potential $\widetilde{W}$, $\widetilde{\bar{W}}$ will be referred to as the transformation potential for the rest of this paper.

For the current application, instead of predicting which interface will form, determining which orientations will

transform first is of interest. Using a 3-1-3 Euler (Bunge) rotation matrix [24, eqn.2.50], where ϕ_1, Φ, and ϕ_2 are the rotation angles from the sample to crystallographic reference frames about the z, x' and z'' axes, respectively, it is possible to rotate the interfaces over all possible crystallographic orientations:

$$\mathbf{Q} = \begin{bmatrix} cos(\phi_1)cos(\phi_2) - sin(\phi_2)cos(\Phi)sin(\phi_1) & cos(\phi_2)sin(\phi_1) + sin(\phi_2)cos(\Phi)cos(\phi_1) & sin(\phi_2)sin(\Phi) \\ -cos(\phi_1)sin(\phi_2) - cos(\phi_2)cos(\Phi)sin(\phi_1) & -sin(\phi_1)sin(\phi_2) + cos(\phi_2)cos(\Phi)cos(\phi_1) & cos(\phi_2)sin(\Phi) \\ sin(\Phi)sin(\phi_1) & -sin(\Phi)cos(\phi_1) & cos(\Phi) \end{bmatrix} \quad (5)$$

Applying this to the available-work criterion gives:

$$W^{(k)}(\phi_1, \Phi, \phi_2) = \mathbf{Q}_{ni}(\phi_1, \Phi, \phi_2) b_i^{(k)} \sigma_{nm} \mathbf{Q}_{mj}(\phi_1, \Phi, \phi_2) \hat{\mathrm{m}}_j^{(k)} \quad (6)$$

The magnitude of the transformation potential $W(\phi_1, \Phi, \phi_2)$ can now be presented in an orientation distribution plot. Considering the whole (ϕ_1, Φ, ϕ_2) orientation space, the larger values for $W(\phi_1, \Phi, \phi_2)$ are the orientations where transformation is likely to occur.

2. Transformation predictions

No data is currently available in the literature for the lattice parameters for martensite in TRIP steels. Using data for conventional steels from [25], the following lattice parameters were calculated based upon 0.1% mass fraction carbon:

$$a_0 = \quad 0.35594\text{nm}\ a' = \quad 0.28657\text{nm}\ c' = \quad 0.28786\text{nm} \quad (7)$$

These values are similar to the lattice parameters used in [16]. The calculated variant volume ratio (λ) for these values is 0.41, which compares well to the value of 0.35 in [16] measured from the ratio of variant width in the twinned structure.

Sixteen different macroscopic stress states will be investigated, listed in Table 1 and illustrated in Fig. 1. The abscissa is set parallel to the rolling direction (RD) and the ordinate parallel to the transverse direction (TD). Each stress state is described by the RD or TD axis that it is nearest to, and the type of forming operation that creates this stress state. To compare the transformation potentials, the different stress states have been normalized using the equation:

$$\sigma_e = \frac{1}{\sqrt{2}}\Big[(\sigma_{11} - \sigma_{22})^2 + (\sigma_{22} - \sigma_{33})^2 + (\sigma_{33} - \sigma_{11})^2 + 6(\tau_{12}^2 + \tau_{23}^2 + \tau_{31}^2)\Big]^{\frac{1}{2}} \quad (8)$$

such that the effective stress (σ_e) is equal to 1 and assuming material isotropy. The resulting stress tensors are shown in Table 1.

For the cubic–orthorhombic symmetry expected for the austenite phase in sheet steels, only the orientations within the $0° \leqslant \phi_1 \leqslant 90°, 0° \leqslant \Phi \leqslant 90°$ and $0° \leqslant \phi_2 \leqslant 90°$ subset of orientation space need to be calculated. A script written in PERL performed these calculations in 5° increments throughout this subset. Fig. 2 shows orientation distribution (OD) plots of the maximum transformation potential $\widetilde{W}$ on $\phi_2 = 45°$ sections, which contains the orientations of interest for FCC materials.

The values of the maximum transformation potential $\widetilde{W}$ calculated in Eq. (6) have also been tabulated in Table 2 for Brass, Copper and Cube orientations. Brass orientations occur in three places in the $0° \leqslant \phi_1 \leqslant 90°, 0° \leqslant \Phi \leqslant 90°$ and $0° \leqslant \phi_2 \leqslant 90°$ subspace: $(\phi_1, \Phi, \phi_2) : (55°, 90°, 45°), (35°, 45°, 0°)$ and $(35°, 45°, 90°)$ that will be referred to as Brass[1], Brass[2], and Brass[3], respectively. Copper orientations occur at two places in $(\phi_1, \Phi, \phi_2) : (90°, 35°, 45°)$ and $(39°, 66°, 27°)$ which will be referred to as Copper[1] and Copper[2]. Data from each of these orientations is included in Table 2. Cube orientations were measured at three locations of (ϕ_1, Φ, ϕ_2): $(0°, 0°, 0°)$, $(90°, 0°, 0°)$ and $(45°, 0°, 45°)$, but were found to be identical, so Table 2 only lists the data from $(\phi_1, \Phi, \phi_2) = (0°, 0°, 0°)$. The maximum and minimum values of $\widetilde{W}$ for the Euler angles investigated are listed in Table 3, as well as the orientations.

As a sensitivity analysis, different values of the austenite and martensite unit cells were calculated, corresponding to 0.01% and 0.25% mass fraction C. The magnitude of the

Table 1
Tensor descriptions of the 16 different stress states investigated. Key to notation: Uniaxial tension along RD (RD-T), plane strain along the RD axis (RD-PS), balanced biaxial tension (BB), plane strain along the TD axis (TD-PS), uniaxial tension along the TD axis (TD-T), deep drawing along the TD axis (TD-DD), pure shear with the TD axis positive (TD-S), extrusion along the RD axis (RD-EX) compression along the RD axis (RD-C). Shrinking along the RD axis (RD-SH), balanced biaxial compression (BB-C), shrinking along the TD axis, compression along the TD axis (TD-C), extrusion along the TD axis (TD-EX), pure shear with the RD axis positive (RD-S), deep drawing along the RD axis (RD-DD).

RD-T $\begin{bmatrix}1&0&0\\0&0&0\\0&0&0\end{bmatrix}$	RD-PS $\begin{bmatrix}\frac{2}{\sqrt{3}}&0&0\\0&\frac{1}{\sqrt{3}}&0\\0&0&0\end{bmatrix}$	BB $\begin{bmatrix}1&0&0\\0&1&0\\0&0&0\end{bmatrix}$	TD-PS $\begin{bmatrix}\frac{1}{\sqrt{3}}&0&0\\0&\frac{2}{\sqrt{3}}&0\\0&0&0\end{bmatrix}$
TD-T $\begin{bmatrix}0&0&0\\0&1&0\\0&0&0\end{bmatrix}$	TD-DD $\begin{bmatrix}-\frac{1}{\sqrt{7}}&0&0\\0&\frac{2}{\sqrt{7}}&0\\0&0&0\end{bmatrix}$	TD-S $\begin{bmatrix}-\frac{1}{\sqrt{3}}&0&0\\0&\frac{1}{\sqrt{3}}&0\\0&0&0\end{bmatrix}$	RD-EX $\begin{bmatrix}-\frac{2}{\sqrt{7}}&0&0\\0&\frac{1}{\sqrt{7}}&0\\0&0&0\end{bmatrix}$
RD-C $\begin{bmatrix}-1&0&0\\0&0&0\\0&0&0\end{bmatrix}$	RD-SH $\begin{bmatrix}-\frac{2}{\sqrt{3}}&0&0\\0&-\frac{1}{\sqrt{3}}&0\\0&0&0\end{bmatrix}$	BB-C $\begin{bmatrix}-1&0&0\\0&-1&0\\0&0&0\end{bmatrix}$	TD-SH $\begin{bmatrix}-\frac{1}{\sqrt{3}}&0&0\\0&-\frac{2}{\sqrt{3}}&0\\0&0&0\end{bmatrix}$
TD-C $\begin{bmatrix}0&0&0\\0&-1&0\\0&0&0\end{bmatrix}$	TD-EX $\begin{bmatrix}\frac{1}{\sqrt{7}}&0&0\\0&-\frac{2}{\sqrt{7}}&0\\0&0&0\end{bmatrix}$	RD-S $\begin{bmatrix}\frac{1}{\sqrt{3}}&0&0\\0&-\frac{1}{\sqrt{3}}&0\\0&0&0\end{bmatrix}$	RD-DD $\begin{bmatrix}\frac{2}{\sqrt{7}}&0&0\\0&-\frac{1}{\sqrt{7}}&0\\0&0&0\end{bmatrix}$

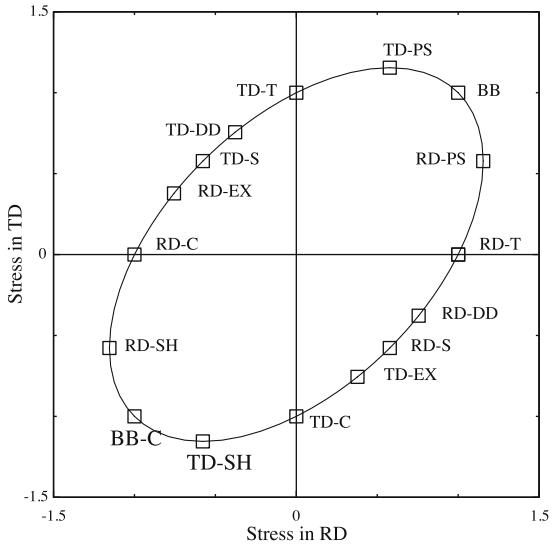

Fig. 1. Stress tensors investigated plotted in the RD–TD plane. Key to notation is described in Table 1.

transformation potential changed slightly, but no significant changes in the orientation distribution plot shape were found. The calculations shown are for the $m3m$ point group. Additional calculations for the $m\bar{3}m$ space group, which allows improper rotations ($\det = -1$) and increases the number of possible interfaces from 24 to 48 were also performed, but the transformation potential values were found to be identical to the $m3m$ point group.

3. Discussion

The data in Tables 2, 3 and Fig. 2 show the significant effects of both stress state and orientation on the transformation potential, and therefore on the ability for austenite to transform into martensite. For TRIP steels, the Brass and Copper orientations are the most common orientations with which grains are found to be aligned [8,9]. For all stress states investigated, the values of the transformation potential for grains aligned with Copper and Brass orientations are lower than cube orientations. Transformation potentials for Copper orientations are generally lower than Brass. This means that, for austenite grains aligned in the cube direction, the shear caused by twinned martensite is closely aligned with the shear direction and plane caused by the different loading conditions. As the values of the transformation potential give a ratio of the stress states required for transformation, this result implies that the grain orientations that are most common are also more difficult to transform for the investigated stress states.

Comparing the RD-T and TD-T $\phi_2 = 45^\circ$ sections, mirror symmetry along $\phi_1 = 45^\circ$ can be seen which occurs due

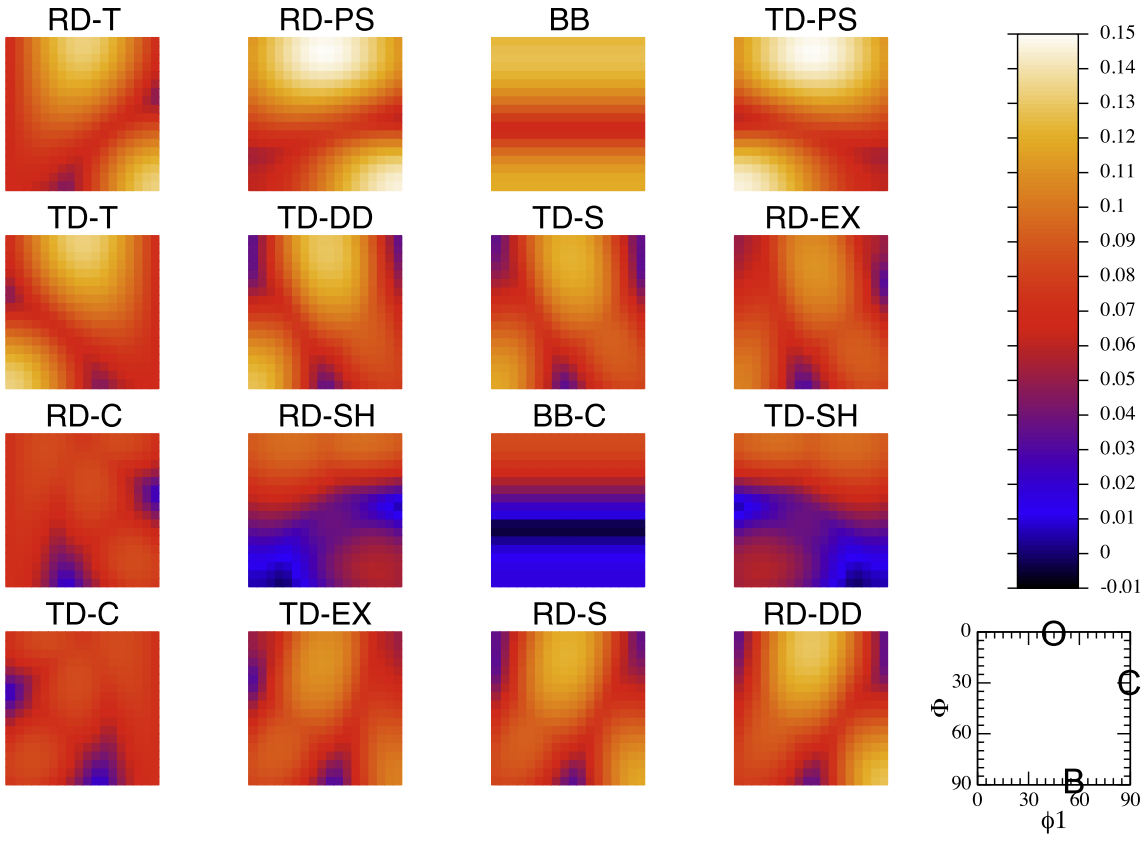

Fig. 2. $\phi_2 = 45^\circ$ orientation distribution sections of transformation potential $\widetilde{W}$ shown for the 16 stress states described in Table 1 and Fig. 1. Cube orientation in this section is marked with an "O" at $(45^\circ, 0^\circ, 45^\circ)$, Copper orientation is marked with a "C" at $(90^\circ, 35^\circ, 45^\circ)$ and Brass orientation is marked with a "B" at $(55^\circ, 90^\circ, 45^\circ)$.

Table 2
Transformation potential $\widetilde{W}$ values for Brass, Copper and Cube orientations.

Domain	Orientation: (ϕ_1, Φ, ϕ_2): $(hkl)\langle uvw\rangle$	Cube (0,0,0) $(001)\langle 100\rangle$	Brass[1] (55,90,45) $(110)\langle 1\bar{1}2\rangle$	Brass[2] (35,45,0) $(011)\langle 2\bar{1}1\rangle$	Brass[3] (35,45,90) $(101)\langle \bar{1}2\bar{1}\rangle$	Copper[1] (90, 35,45) $(112)\langle \bar{1}\bar{1}1\rangle$	Copper[2] (39,66,27)* $(121)\langle 1\bar{1}1\rangle$
1	RD-T	0.1325	0.0887	0.0887	0.0887	0.0398	0.0405
	RD-PS	0.1467	0.1198	0.1198	0.1198	0.0834	0.0854
	BB	0.1215	0.1188	0.1188	0.1188	0.1046	0.1079
	TD-PS	0.1467	0.0909	0.0909	0.0909	0.0978	0.1014
	TD-T	0.1325	0.0398	0.0398	0.0398	0.0648	0.0678
2	TD-DD	0.1278	0.0513	0.0513	0.0513	0.0535	0.0548
	TD-S	0.1187	0.0554	0.0554	0.0554	0.0442	0.0452
	RD-EX	0.1054	0.0575	0.0575	0.0575	0.0334	0.0339
3	RD-C	0.0731	0.0562	0.0562	0.0562	0.0133	0.0142
	RD-SH	0.0908	0.0419	0.0419	0.0419	0.0233	0.0246
	BB-C	0.0841	0.0164	0.0164	0.0164	0.0403	0.0413
	TD-SH	0.0908	0.0163	0.0163	0.0163	0.0639	0.0648
	TD-C	0.0731	0.0133	0.0133	0.0133	0.0704	0.0719
4	TD-EX	0.1054	0.0386	0.0386	0.0386	0.0678	0.0687
	RD-S	0.1187	0.0512	0.0512	0.0512	0.0630	0.0635
	RD-DD	0.1278	0.0620	0.0620	0.0620	0.0558	0.0560

* Measured at: (40,65,25).

Table 3
Orientations of the maximum and minimum transformation potential $\widetilde{W}$ for each stress state.

Domain	Stress state	Maximum		Minimum	
		Orientation	Value	Orientation	Value
1	RD-T	(5,35,85)	0.1331	(45,55,15)	0.0397
	RD-PS	(10,20,80)	0.1536	(0,70,45)	0.0516
	BB	(20,20,10)	0.1330	(70,55,45)	0.0617
	TD-PS	(80,20,10)	0.1536	(90,70,45)	0.0516
	TD-T	(85,35,5)	0.1331	(45,55,75)	0.0397
2	TD-DD	(85,20,0)	0.1323	(0,15,45)	0.0270
	TD-S	(90,20,5)	0.1254	(90,20,45)	0.0236
	RD-EX	(90,20,5)	0.1140	(50,45,0)	0.0211
3	RD-C	(25,60,80)	0.0847	(45,55,15)	0.0131
	RD-SH	(60,5,50)	0.0975	(20,90,45)	−0.0043
	BB-C	(15,5,20)	0.0844	(30,55,45)	−0.0086
	TD-SH	(30,5,40)	0.0975	(20,45,0)	−0.0043
	TD-C	(65,60,10)	0.0847	(45,55,75)	0.0131
4	TD-EX	(0,20,85)	0.1140	(40,45,0)	0.0211
	RD-S	(0,20,5)	0.1254	(0,20,45)	0.0236
	RD-DD	(5,20,0)	0.1323	(90,15,45)	0.0270

to symmetry of the Bunge Euler angles. Symmetry is observed in all RD-X and TD-X loading conditions, where X is a type of loading (T, C, PS, etc.). The orientations for the maximum and minimum transformation potential in Table 3 show this symmetry. Cube, and any other orientations along the $\phi_1 = 45^\circ$, $\phi_2 = 45^\circ$ line, will be the same for both RD-X and TD-X loading conditions. The transformation potentials for the Brass or Copper orientations will not be symmetric between RD-X and TD-X because the Brass and Copper orientations do not fall along the $\phi_1 = 45^\circ$, $\phi_2 = 45^\circ$ line.

The $90^\circ \times 90^\circ \times 90^\circ$ orientation space explored here is valid for cubic crystal symmetry and orthotropic sample symmetry expected in sheet metals, and contains expected redundancy of the Copper, Brass and Cube orientations within this space. There is some variation between the transformation potential value $\widetilde{W}$ for the Copper components, this but may be due to the slight misorientation between the true orientation and measured orientation. Brass orientations have the same value regardless of where they are measured, indicating this is not a computational artifact.

For further discussion, the stress states are separated into four domains: domain 1 containing the stress states in the positive–positive quadrant from RD-T to TD-T; domain 2 the negative–positive quadrant with stress states TD-DD, TD-S and RD-EX; domain 3 considering the negative–negative quadrant from RD-C to TD-C; and finally domain 4 with TD-EX, RD-S and RD-DD.

3.1. Domain 1

For the RD-T stress state, the locations of the lowest transformation potential are close to the Copper orientations. As shown in Table 2, the Brass orientation has approximately twice the value of the Copper orientation. Also, the Cube texture potential value is three times the Copper orientation value. Thus, for tension along the rolling direction and a stress level that will transform austenite oriented with the Cube orientation ($\sigma = \sigma_T$), grains aligned with the Copper orientation would require a stress level of $\approx 3\sigma_T$ to transform, and grains aligned with the Brass orientation would require $\approx 1.5\sigma_T$.

Similar behavior is seen in the TD-T stress state. The OD plots are mirror images due to the symmetry in Bunge notation. In this stress state the Copper and Brass orientations exhibit transformation potentials that are much lower than

the Cube orientation, and are comparable to the values of the Copper orientation in the RD-T stress state. In this case the minimum in the TD-T stress state is near the transformation potential values of the Brass orientation, which has a lower transformation potential than Copper. While the RD-T stress state had a relatively high value for the transformation potential in the Brass orientation, neither the transformation potentials for Brass nor Copper orientations are high in the TD-T stress state. Transformation in the Brass orientations would require larger stresses in the TD-T stress state than in the RD-T stress state, but lower stresses in the Copper orientation than the RD-T stress state.

The general orientation behavior in the RD-PS and TD-PS stress states are quite similar to the RD-T and TD-T stress states, respectively. The transformation potential has a larger magnitude overall, and the locations of the minima have been shifted and stretched along the ϕ_1 axis. In the Copper orientations the transformation potential values in RD-PS are double the transformation potential values in the RD-T stress state. In the TD-PS stress state the Brass orientation is nearly doubled compared to TD-T stress state. The plane-strain tests have the highest maximum transformation potential value for any of the stress states investigated, as seen in Table 3, with the value for cube orientation (shown in Table 2) very close to this maximum value (shown in Table 3).

The transformation potential in the BB stress state is quite different from either the RD-T and TD-T. The minimum potential occurs along a strip near $\Phi = 55°$, which is referred to as the γ-fiber with the $\{1\,1\,1\}$ plane parallel to the sample normal direction. For the RD-T, TD-T and BB stress states, the maximum transformation potentials are nearly identical, but the value for Cube orientation in this stress state is less than those in the RD-T and TD-T stress states. The values are similar to the Cube orientation because the Brass and Copper orientations do not lie on the γ-fiber. The value for transformation potential in the Brass orientation is less than that seen in the RD-PS case, but the value for Copper orientation is higher than any other stress state investigated.

For all stress states investigated, the cube orientation has the highest transformation potential in either PS stress state. Similarly, the highest overall transformation potential for the Brass orientation occurs in the RD-PS case, and for grains aligned with the Copper orientation the highest transformation potential value overall is in the BB stress state. In domain 1, the lowest value for the Cube orientation occurs in the BB stress state; for Brass, the TD-T stress state; and for Copper the RD-T stress state. The transformation potential for the Copper orientations are higher than Brass only for the TD-PS and TD-T stress states.

3.2. Domain 2

All of the stress states discussed thus far have been in the positive–positive quadrant of stress space, where most forming operations typically occur. Domain 2 contains deep drawing (TD-DD), pure shear (TD-S) and extrusion (RD-EX) stress states, which also can be encountered in production. For each of these stress states the transformation potential for each component has similar values and shape. The shape is similar to the TD-T stress state with some stretching along the Φ axis. The Cube orientation value is twice as large as that of the Brass or Copper orientations. As the stress state changes from TD-DD to TD-S to RD-EX the value of the transformation potential for Cube and Copper orientations decreases while the transformation potential for Brass orientation increases slightly.

3.3. Domain 3

Domain 3, which deals with the negative–negative quadrant, is quite different than the preceding domains. Following the stress-space arc in domains 1 and 2 from RD-T to RD-EX there is a clear progression in the trends of the transformation potential. This changes in the RD-C case, which does not continue the shape of RD-EX, but rather resets to be similar to the RD-T stress state. There is a correlation between the orientation distribution shape between the domain 1 and domain 3 stress states. The values for the transformation potential are much lower in this domain than others, but are generally still positive, indicating transformation will occur in compression.

Much like domain 1, the RD-C and TD-C stress states have the same values for the Cube orientation. For RD-C stress state the Brass orientation is of a similar magnitude to the Cube orientation, and the Copper orientation is much lower. For TD-C stress state the behavior is reversed, the Copper orientation is of similar magnitude to the Cube orientation and the Brass orientation is much lower, as seen in their tensile counterparts. For these two stress states the minimum value is still positive, indicating that transformation is possible for any orientation at high enough stress.

This is not the case for the RD-SH, BB-C and TD-SH stress states, where there are some orientations where the transformation potential for that orientation is a negative value. That implies that in these orientations transformation will never occur, regardless of the applied stress. For the BB-C stress state the transformation potential for Brass orientations is approximately one-sixth of the Cube values and for Copper orientations a third of the cube values. The BB-C stress state also has the lowest maximum and minimum values of any of the investigated stress states. The RD-SH and TD-SH stress states have the same values for the cube orientation, but the Brass and Copper orientations are quite different. In the RD-SH stress state, the transformation potential for Copper orientations are half that of Brass, in the TD-SH the Brass orientation is a quarter of the Copper orientation value.

3.4. Domain 4

The transformation potentials for stress states TD-EX, RD-S and RD-DD in domain 4 are similar to the stress states

in domain 2. The transformation potential values for maximum, minimum and Cube orientations in deep drawing (DD), pure shear (S) and extrusion (EX) stress states are the same for either RD or TD values. In contrast to domain 2, the Copper orientations are much higher in this domain while the Brass orientations vary more significantly.

3.5. Summary

For an as-received TRIP steel, typically hot-rolled, the austenite texture will be primarily composed of Brass- or Copper-oriented grains. From the data in Table 2 and Fig. 2, it is clear that these orientations correspond to low values of the transformation potential. Cube orientations, the recrystallization texture, have the high values of transformation potential for all stress states investigated. From a processing point of view this implies that the Brass and Copper orientations may not be favorable, because the applied stress state may never reach the levels required to transform the austenite in these regions. This may explain the retained austenite observed in the microstructure of several experimental studies [15,26]. There is a line of mirror symmetry between RD-X and TD-X stress states, but this does not imply that the values of the transformation potential will be the same for the same crystallographic orientations. The mirror symmetry is observed in the overall maximum, overall minimum and Cube orientation values, but not the Brass or Copper orientations.

There is clear asymmetry in the transformation potential between the tensile and compressive stress states, implying that the hardening behavior will not be completely isotropic. The additional effects of microstructural stresses are not included in this analysis, but assuming they are known, could be easily added to the stress states presented. Only the stress state and lattice parameters have been included in this model, so the results of this analysis should be valid for any stress-induced austenite to twinned martensite transformation. One use of this analysis may be optimization of the texture components for transformation by either distributing the textures so that the transformation occurs evenly for a given stress state, ensuring all of the austenite will be transformed by the end of a forming process, or delaying the start of transformation until a specified stress value has been reached.

4. Conclusion

The effects of orientation and stress state on the austenite to martensite phase transformation in TRIP steels were investigated in this work. Twinned martensite structures were calculated using the CTM. An available-work criterion was used to predict the transformation potentials for 16 different stress states. By rotating the twinned martensite structures over all crystallographic orientations using Euler angles, the magnitude of the transformation potential was plotted as an orientation distribution plot. From these data, the Brass and Copper orientation components that are typical in as-processed TRIP steels were found to correspond to low values of the transformation potential. Grains aligned with these orientations would require higher stresses to transform than other orientations, and may therefore never transform.

Acknowledgments

The authors thank T.W. Shield for use of his CTM-0.0.1 program; Steve Banovic, Thomas Gnäupel-Herold, Mark Iadicola and Mark Stoudt at the Center for Metal Forming at NIST for advice and assistance; and the Research Associate Program at the National Academies for supporting this work.

References

[1] Committee on Automotive Applications. Advanced high strength steel (AHSS) application guidelines version 4.0. http://www.worldautosteel.org. International Iron & Steel Institute; 2009.
[2] Zackay V, Parker E, Fahr D, Busch R. ASM Trans Quart 1967;60:252.
[3] Fischer F, Reisner G, Werner E, et al. Int J Plast 2000;16:723.
[4] Bhadeshia HKDH. Iron Steel Inst Jpn 2002;42:1059.
[5] Jacques P. Curr Opin Solid State Mater Sci 2004;8:259.
[6] Girault E, Mertens A, Jacques P, et al. Scripta Mater 2001;44:885.
[7] Guo L. Master's thesis, Pohang University of Science and Technology; 2007.
[8] Wasilkowska A, Petrov R, Kestens L, et al. ISIJ Int 2006;46:302.
[9] He Y, Godet S, Jacques P, Jonas J. Mater Sci Forum 2005;495–497:345.
[10] Kocks UF, Tomé CN, Wenk H-R, editors. Texture and anisotropy. Cambridge: Cambridge University Press; 1998.
[11] Hutchinson B, Ryde L, Lindh E, Tagashira K. Mater Sci Eng A 1998;257:9.
[12] Hane KF. Ph.D. thesis, University of Minnesota; 1998.
[13] Tsakiris V, Edmonds DV. Mater Sci Eng A 1999;273–275:430.
[14] Petein A, Ryelandt L, Godet S, Jacques P. Mater Sci Forum 2005;495–497:459.
[15] Van Rompaey T, Lani F, Jacques P, et al. Metall Mater Trans A 2006;37:99.
[16] Zhang MX, Kelly PM, Gates JD. Mater Sci Eng A 1999;273–275:251.
[17] Ball JM, James RD. Arch Rational Mech Anal 1987;100:13.
[18] Bhattacharya K. Microstructure of martensite. Oxford: Oxford University Press; 2003.
[19] He Y, Godet S, Jacques PJ, Jonas JJ. Metall Mater Trans A 2006;37:2641.
[20] Shield TW. CTM-0.0.1. University of Minnesota; 2005.
[21] Shield TW. J Mech Phys Solids 1995;43:869.
[22] Vasko GM, Leo PH, Shield TW. J Mech Phys Solids 2002;50:1843.
[23] Creuziger A, Crone WC. Acta Mater 2008;56:518.
[24] Bunge H-J. Texture analysis in materials science: mathematical methods. London: Butterworth; 1982.
[25] Jatczak CF, Larson JA, Shin SW. Retained austenite and its measurements by X-ray diffraction; an information manual (SAE SP453). Society of Automotive Engineers; 1980.
[26] Jacques P, Furnmont Q, Lani F, et al. Acta Mater 2007;55:3681.